

Dynamics of Learning with Restricted Training Sets

II. Tests and Applications

A.C.C. Coolen

Department of Mathematics
King's College London
Strand, London WC2R 2LS, UK

D. Saad

The Neural Computing Research Group
Aston University
Birmingham B4 7ET, UK

September 28th 1999

Abstract

We apply a general theory describing the dynamics of supervised learning in layered neural networks in the regime where the size p of the training set is proportional to the number of inputs N , as developed in a previous paper, to several choices of learning rules. In the case of (on-line and batch) Hebbian learning, where a direct exact solution is possible, we show that our theory provides exact results at any time in many different verifiable cases. For non-Hebbian learning rules, such as Perceptron and AdaTron, we find very good agreement between the predictions of our theory and numerical simulations. Finally, we derive three approximation schemes aimed at eliminating the need to solve a functional saddle-point equation at each time step, and assess their performance. The simplest of these schemes leads to a fully explicit and relatively simple non-linear diffusion equation for the joint field distribution, which already describes the learning dynamics surprisingly well over a wide range of parameters.

PACS: 87.10.+e, 02.50.-r, 05.20.-y

Contents

1	Introduction	2
2	Summary of the Theory and its Properties	3
2.1	The Macroscopic Laws	3
2.2	Properties of the Macroscopic Laws	4
3	Benchmark Tests: Hebbian Learning	6
3.1	Batch Hebbian Learning	7
3.2	On-Line Hebbian Learning	8
4	General Approximation Schemes	14
4.1	Large α Approximation	14
4.2	Conditionally-Gaussian Approximation	15
4.3	Partially Annealed Approximation	16
5	Non-Hebbian Rules: Theory versus Simulations	17
5.1	Large α and Conditionally-Gaussian Approximations	18
5.2	Partially Annealed Approximation and Full Equations	23
6	Discussion	26

1 Introduction

In a previous paper [1] we have applied the formalism of dynamical replica theory [2] to analyse the dynamics of supervised learning in perceptrons with restricted training sets. For an introduction into the area of the dynamics of learning in layered neural networks, a guide to the relevant references, as well as a proper discussion of the peculiarities of the dynamics of learning with restricted as opposed to infinite training sets, we refer to [1]. The microscopic variables in the learning process are the components of the weight vector \mathbf{J} of the ‘student’ network. The ‘teacher’ network, which defines the task to be learned by the student, is characterised by a weight vector \mathbf{B} . Learning proceeds on the basis of answers to be given to questions $\boldsymbol{\xi} \in \tilde{D} \subseteq \{-1, 1\}^N$, according to a dynamical rule for \mathbf{J} which is defined in terms of a function $\mathcal{G}[x, y]$, where $x = \mathbf{J} \cdot \boldsymbol{\xi}$ and $y = \mathbf{B} \cdot \boldsymbol{\xi}$ are the student and teacher fields, respectively. The randomly composed set \tilde{D} of questions, of size $p = \alpha N$, is called the training set. If $\alpha < \infty$ as $N \rightarrow \infty$ the learning dynamics will be nontrivial. Firstly, the data in \tilde{D} will be recycled in due course, which generates complicated correlations and non-Gaussian local field distributions, and allows the system to improve its performance partly by memorizing answers rather than by learning the underlying rule (hence the difference between training- and generalization errors). Secondly, the actual composition of the randomly drawn training set introduces an element of frozen disorder into the problem, which will have to be averaged out. The analysis described in [1] resulted in a general macroscopic theory, describing the behaviour of such learning processes with $\alpha < \infty$ in the limit $N \rightarrow \infty$ (infinite systems) and on finite time-scales, in terms of deterministic laws for macroscopic observables. The theory applies to both on-line learning (where weight updates are made after each presentation of an input vector from the training set), and to batch learning (where weight updates are themselves averages over the full training set), as well as to arbitrary learning rules (i.e. arbitrary functions $\mathcal{G}[x, y]$).

In this paper we apply this general theory to various different specific choices of learning rules. One of these, (on-line and batch) Hebbian learning, provides an excellent benchmark test for our theory, since for this simple rule exact solutions are known, even for the regime of restricted training sets [4]. We find that our theory is fully exact for batch execution, and that it succeeds in predicting exactly the evolution of several macroscopic observables, including the generalisation error and moments of the joint field distribution for student and teacher fields, in the on-line case (although here full exactness is difficult to assess, and not a priori guaranteed). A preliminary presentation of some of the results in this paper (those involving Hebbian learning) was given in [3]. For non-Hebbian error-correcting learning rules, such as on-line and batch versions of Perceptron learning and AdaTron learning, no exact solutions are known at present with which to confront our theory; instead we here compare the predictions (with regard to the evolution of training- and generalization errors and the joint field distribution) of the full theory, as well as of a number of simple approximations of our equations, with the results of carrying out extensive numerical simulations in large (size $N = 10,000$) neural networks. We find, surprisingly, that even the simplest of these approximations, which does not require solving any saddle point equations and takes the form of a fully explicit non-linear diffusion equation for the joint field distributions $P[x, y]$, describes the simulation experiments remarkably well. Employing the more sophisticated (and thereby more CPU intensive) approximations, or, at the other end of the spectrum, a numerical solution of the full macroscopic theory, leads to increasingly accurate quantitative predictions for the evolution of the relevant macroscopic observables of the learning process, with deviations between theory and numerical experiment which are of the order of magnitude of the finite size effects in the simulations. We close our paper with a discussion of the strengths and weaknesses of the approach used, and an outlook on future work on the dynamics of

learning with restricted training sets, involving the present and possibly other formalisms.

2 Summary of the Theory and its Properties

In this section we will be brief in order to avoid inappropriate duplication of the material in [1], to which we refer for full details.

2.1 The Macroscopic Laws

Our macroscopic observables are $Q = \mathbf{J}^2$, $R = \mathbf{B} \cdot \mathbf{J}$, and the joint distribution of student and teacher fields (or ‘activations’) $P[x, y] = \langle \delta[x - \mathbf{J} \cdot \boldsymbol{\xi}] \delta[y - \mathbf{B} \cdot \boldsymbol{\xi}] \rangle_{\tilde{D}}$. For $N \rightarrow \infty$ all these quantities are found to obey deterministic and self-averaging equations. We define $\langle f[x, y] \rangle = \int dx Dy P[x|y] f[x, y]$, where $Dy = (2\pi)^{-\frac{1}{2}} e^{-\frac{1}{2}y^2} dy$, and the following averages (the function $\Phi[x, y]$ will be specified below):

$$U = \langle \Phi[x, y] \mathcal{G}[x, y] \rangle \quad V = \langle x \mathcal{G}[x, y] \rangle \quad W = \langle y \mathcal{G}[x, y] \rangle \quad Z = \langle \mathcal{G}^2[x, y] \rangle \quad (1)$$

For on-line learning (which is a stochastic process) we have found, using the prescriptions of dynamical replica theory (in replica symmetric ansatz) [1]:

$$\begin{aligned} \frac{d}{dt} Q &= 2\eta V + \eta^2 Z & \frac{d}{dt} R &= \eta W \\ \frac{d}{dt} P[x|y] &= \frac{1}{\alpha} \int dx' P[x'|y] [\delta[x - x' - \eta \mathcal{G}[x', y]] - \delta[x - x']] - \eta \frac{\partial}{\partial x} \left\{ P[x|y] [U(x - Ry) + Wy] \right\} \\ &+ \frac{1}{2} \eta^2 Z \frac{\partial^2}{\partial x^2} P[x|y] - \eta \left[V - RW - (Q - R^2)U \right] \frac{\partial}{\partial x} \left\{ P[x|y] \Phi[x, y] \right\} \end{aligned} \quad (2)$$

For batch learning (which is a deterministic process) we found:

$$\begin{aligned} \frac{d}{dt} Q &= 2\eta V & \frac{d}{dt} R &= \eta W \\ \frac{d}{dt} P[x|y] &= -\frac{\eta}{\alpha} \frac{\partial}{\partial x} [P[x|y] \mathcal{G}[x, y]] - \eta \frac{\partial}{\partial x} \left\{ P[x|y] [U(x - Ry) + Wy] \right\} \\ &- \eta \left[V - RW - (Q - R^2)U \right] \frac{\partial}{\partial x} \left\{ P[x|y] \Phi[x, y] \right\} \end{aligned} \quad (4)$$

From the solution of the above closed sets of equations for the trio $\{Q, R, P\}$ (one of which is a function) follow the familiar training- and generalization errors $E_t = \langle \theta[-xy] \rangle$ and $E_g = \pi^{-1} \arccos[R/\sqrt{Q}]$. The auxiliary order parameters generated in the replica calculation, the spin-glass order parameter q and the function $M[x|y]$, are calculated at each time-step by solving the following saddle-point equations:

$$\langle (x - Ry)^2 \rangle + (qQ - R^2)(1 - \frac{1}{\alpha}) = \left[2(qQ - R^2)^{\frac{1}{2}} + \frac{1}{B} \right] \int Dy Dz z \langle x \rangle_{\star} \quad (6)$$

$$P[X|y] = \int Dz \langle \delta[X - x] \rangle_{\star} \quad (7)$$

with

$$B = \frac{\sqrt{qQ - R^2}}{Q(1 - q)} \quad \langle f[x, y, z] \rangle_{\star} = \frac{\int dx M[x|y] e^{Bxz} f[x, y, z]}{\int dx M[x|y] e^{Bxz}} \quad (8)$$

Without loss of generality we can always normalize M according to $\int dx M[x|y] = 1$ for all $y \in \mathfrak{R}$. From the physical meaning of q follows $R^2/Q \leq q \leq 1$. After q and $M[x|y]$ have been determined, the key function $\Phi[x|y]$ in (1,3,5) is calculated as

$$\Phi[X|y] = \left\{ Q(1-q)P[X|y] \right\}^{-1} \int Dz \langle X-x \rangle_\star \langle \delta[X-x] \rangle_\star \quad (9)$$

We refer to [1] for full derivations of the above equations.

2.2 Properties of the Macroscopic Laws

Some useful properties of our theory are independent of which learning rule $\mathcal{G}[x|y]$ is used. The first of these is that in the limit $\alpha \rightarrow \infty$, which corresponds to the case of infinite training sets, our theory reduces to the simpler formalism initiated in [5] and elaborated in papers like [6, 7], which is built on assuming $P[x|y]$ to be of a Gaussian form (this only happens as $\alpha \rightarrow \infty$) [1]. Secondly, for any given q the solution $M[x|y]$ of the functional saddle-point problem (7) is unique, and can even be obtained as the fixed-point of a converging nonlinear functional map [1]. Thirdly, we note that the first conditional moment $\bar{x}(y) = \int dx x P[x|y]$ of $P[x|y]$ of the joint field distribution obeys a simple equation, which is obtained from (3) and (5) upon multiplication by x , followed by integration over x :

$$\frac{d}{dt} [\bar{x}(y) - Ry] = \frac{\eta}{\alpha} \int dx P[x|y] \mathcal{G}[x|y] + \eta U[\bar{x}(y) - Ry] \quad (10)$$

where we have also used the built-in property $\int dx P[x|y] \Phi[x|y] = 0$ for all y .

Alternatively we could rewrite our macroscopic equations into Fourier language, i.e. in terms of $\hat{P}[k|y] = \int dx e^{-ikx} P[x|y]$ and $\hat{M}[k|y] = \int dx e^{-ikx} M[x|y]$. The functional saddle-point equation, giving $\hat{M}[k]$, then becomes

$$\hat{P}[k|y] = \int Dz \frac{\hat{M}[k+iBz|y]}{\hat{M}[iBz|y]} \quad (11)$$

and the diffusion equation takes the form

$$\begin{aligned} \frac{d}{dt} \log \hat{P}[k|y] &= \frac{1}{\alpha} \left\{ \int dk' \frac{\hat{P}[k'|y]}{\hat{P}[k|y]} \int \frac{dx'}{2\pi} e^{ix'(k'-k) - i\eta k \mathcal{G}[x',y]} - 1 \right\} - i\eta k (W - UR)y \\ &+ \eta k U \frac{\partial}{\partial k} \log \hat{P}[k|y] - \frac{1}{2} \eta^2 k^2 Z - i\eta k \left[\frac{V - RW - (Q - R^2)U}{\sqrt{qQ - R^2} \hat{P}[k|y]} \right] \int Dz z \frac{\hat{M}[k+iBz|y]}{\hat{M}[iBz]} \end{aligned} \quad (12)$$

This representation will be particularly convenient when applying our theory to Hebbian learning rules. We can derive more explicit results for the special class of locally Gaussian solutions, defined as

$$P[x|y] = \frac{e^{-\frac{1}{2}[x-\bar{x}(y)]^2/\Delta^2(y)}}{\Delta(y)\sqrt{2\pi}}$$

For such distributions the functional saddle-point equation (7) can be solved, giving

$$M[x|y] = \frac{e^{-\frac{1}{2}[x-\bar{x}(y)]^2/\sigma^2(y)}}{\sigma(y)\sqrt{2\pi}} \quad (13)$$

with $\Delta^2(y) = \sigma^2(y) + B^2\sigma^4(y)$. For such solutions to exist, the conditional moments $\bar{x}(y)$ and $\Delta(y)$ must obey the following equation:

$$\begin{aligned} -ik \frac{d}{dt} \bar{x}(y) - \frac{1}{2} k^2 \frac{d}{dt} \Delta^2(y) &= \frac{1}{\alpha} \left\{ \int \frac{du}{\sqrt{2\pi}} e^{-\frac{1}{2}[u-ik\Delta(y)]^2 - ik\eta\mathcal{G}[\bar{x}(y) + u\Delta(y), y]} - 1 \right\} - i\eta k \{W y + U[\bar{x}(y) - R y]\} \\ &\quad - \frac{1}{2} k^2 \left\{ \eta^2 Z + 2\eta U \Delta^2(y) + 2\eta\sigma^2(y) \left[\frac{V - RW - (Q - R^2)U}{Q(1-q)} \right] \right\} \end{aligned} \quad (14)$$

The simple form of (13) allows us to calculate many objects explicitly. In particular:

$$\langle x \rangle_\star = \bar{x}(y) + zB\sigma^2(y) \quad \Phi[x, y] = \frac{x - \bar{x}(y)}{Q(1-q)[1 + B^2\sigma^2(y)]}$$

Finally, for many types of learning rules there are symmetry properties of our macroscopic equations to be exploited. Note that in the most common types of learning rules no distinction is being made between system errors of the type $\{x > 0, y < 0\}$ and those where $\{x < 0, y > 0\}$. This translates into the following property of the function $\mathcal{G}[x, y]$ (note that by the nature of the learning processes under study $\mathcal{G}[x, y]$ can depend on y only via $\text{sgn}(y)$):

$$\mathcal{G}[x, y] = \text{sgn}(y) \left\{ \theta[xy]\mathcal{G}_+ [|x|] + \theta[-xy]\mathcal{G}_- [|x|] \right\} \quad (15)$$

In particular we find for the most common learning recipes:

$$\begin{aligned} \text{Hebbian :} \quad \mathcal{G}_+[u] &= 1, \quad \mathcal{G}_-[u] = 1 \\ \text{Perceptron :} \quad \mathcal{G}_+[u] &= 0, \quad \mathcal{G}_-[u] = 1 \\ \text{AdaTron :} \quad \mathcal{G}_+[u] &= 0, \quad \mathcal{G}_-[u] = u \end{aligned}$$

The form (15) implies the symmetry $\mathcal{G}[-x, y] = \mathcal{G}[x, -y]$, which turns out to allow for self-consistent solutions of the macroscopic equations with the following property at any time:

$$P[-x|y] = P[x| - y] \quad (16)$$

Combination of (16) with (7) and (9) shows that the measure $M[x|y]$ and the function $\Phi[x, y]$ must consequently have the following symmetry properties:

$$M[-x|y] = M[x| - y], \quad \Phi[-x, y] = -\Phi[x, -y]$$

This, in turn, guarantees that the right-hand sides of equations (3) and (5) indeed preserve the symmetry (16) of the field distribution, as claimed.

3 Benchmark Tests: Hebbian Learning

In the special case of the Hebb rule, $\mathcal{G}[x, y] = \text{sgn}[y]$, where weight changes $\Delta \mathbf{J}$ never depend on \mathbf{J} , one can write down an explicit expression for the weight vector \mathbf{J} at any time, and thus for the expectation values of our observables. We choose as our initial field distribution a simple Gaussian one, resulting from an initialization process which did not involve the training set:

$$P_0[x|y] = \frac{e^{-\frac{1}{2}(x-R_0y)^2/(Q_0-R_0^2)}}{\sqrt{2\pi(Q_0-R_0^2)}} \quad (17)$$

Careful averaging of the exact expressions for our observables over all ‘paths’ $\{\xi(0), \xi(1), \dots\}$ taken by the question/example vector through the training set \tilde{D} (for on-line learning), followed by averaging over all realizations of the training set \tilde{D} of size $p = \alpha N$, and taking the $N \rightarrow \infty$ limit, then leads to the following *exact* result [4]. For on-line Hebbian learning one ends up with:

$$Q = Q_0 + 2\eta t R_0 \sqrt{\frac{2}{\pi}} + \eta^2 t + \eta^2 t^2 \left[\frac{1}{\alpha} + \frac{2}{\pi} \right] \quad R = R_0 + \eta t \sqrt{\frac{2}{\pi}} \quad (18)$$

$$P[x|y] = \int \frac{d\hat{x}}{2\pi} e^{-\frac{1}{2}\hat{x}^2[Q-R^2]+i\hat{x}[x-Ry]+\frac{t}{\alpha}[e^{-i\eta\hat{x}} \text{sgn}[y]-1]} \quad (19)$$

For batch learning a similar calculation¹ gives:

$$Q = Q_0 + 2\eta t R_0 \sqrt{\frac{2}{\pi}} + \eta^2 t^2 \left[\frac{1}{\alpha} + \frac{2}{\pi} \right] \quad R = R_0 + \eta t \sqrt{\frac{2}{\pi}} \quad (20)$$

$$P[x|y] = \frac{e^{-\frac{1}{2}[x-Ry-(\eta t/\alpha) \text{sgn}[y]]^2/(Q-R^2)}}{\sqrt{2\pi(Q-R^2)}} \quad (21)$$

Neither of the two field distributions is of a fully Gaussian form (although the batch distribution is at least conditionally Gaussian). Note that for both on-line and batch Hebbian learning we have

$$\int dx x P[x|y] = Ry + \frac{\eta t}{\alpha} \text{sgn}[y] \quad (22)$$

The generalization- and training errors are, as before, given in terms of the above observables as $E_g = \pi^{-1} \arccos[R/\sqrt{Q}]$ and $E_t = \int Dy dx P[x|y] \theta[-xy]$. We thus have exact expressions for both the generalization error and the training error at any time and for any α . The asymptotic values, for both batch and on-line Hebbian learning, are given by

$$\lim_{t \rightarrow \infty} E_g = \frac{1}{\pi} \arccos \left[\frac{1}{\sqrt{1 + \pi/2\alpha}} \right] \quad (23)$$

$$\lim_{t \rightarrow \infty} E_t = \frac{1}{2} - \frac{1}{2} \int Dy \text{erf} \left[|y| \sqrt{\frac{\alpha}{\pi}} + \frac{1}{\sqrt{2\alpha}} \right] \quad (24)$$

As far as E_g and E_t are concerned, the differences between batch and on-line Hebbian learning are confined to transients. Clearly, the above exact results (which can only be obtained for Hebbian-type learning rules) provide excellent and welcome benchmarks with which to test general theories such as the one investigated in the present paper.

¹Note that in [4] only the on-line calculation was carried out; the batch calculation can be done along the same lines.

3.1 Batch Hebbian Learning

We compare the exact solutions for Hebbian learning to the predictions of our general theory, turning first to batch Hebbian learning. We insert into the equations of our general formalism the Hebbian recipe $\mathcal{G}[x, y] = \text{sgn}[y]$. This simplifies our dynamic equations enormously. In particular we obtain:

$$U = 0, \quad V = \langle x \text{ sgn}(y) \rangle, \quad W = \sqrt{2/\pi}$$

For batch learning we consequently find:

$$\begin{aligned} \frac{d}{dt}Q &= 2\eta V & \frac{d}{dt}R &= \eta\sqrt{2/\pi} \\ \frac{d}{dt}P[x|y] &= -\frac{\eta}{\alpha} \text{ sgn}(y) \frac{\partial}{\partial x}P[x|y] - \eta y \sqrt{\frac{2}{\pi}} \frac{\partial}{\partial x}P[x|y] - \eta(V - R\sqrt{\frac{2}{\pi}}) \frac{\partial}{\partial x} \left\{ P[x|y]\Phi[x, y] \right\} \end{aligned}$$

Given the initial field distribution (17), we immediate obtain $V_0 = R_0\sqrt{2/\pi}$. From the general property $\int dx P[x|y]\Phi[x, y] = 0$ and the above diffusion equation for $P[x|y]$ we derive an equation for the quantity $V = \langle x \text{ sgn}(y) \rangle$, resulting in $\frac{d}{dt}V = \eta/\alpha + 2\eta/\pi$, which subsequently allows us to solve

$$Q = Q_0 + 2\eta t R_0 \sqrt{\frac{2}{\pi}} + \eta^2 t^2 \left[\frac{1}{\alpha} + \frac{2}{\pi} \right] \quad R = R_0 + \eta t \sqrt{\frac{2}{\pi}} \quad (25)$$

Furthermore, it turns out that the above diffusion equation for $P[x|y]$ meets the requirements for having conditionally-Gaussian solutions, i.e.

$$P[x|y] = \frac{e^{-\frac{1}{2}[x-\bar{x}(y)]^2/\Delta^2(y)}}{\Delta(y)\sqrt{2\pi}}, \quad M[x|y] = \frac{e^{-\frac{1}{2}[x-\bar{x}(y)]^2/\sigma^2(y)}}{\sigma(y)\sqrt{2\pi}}$$

provided the y -dependent average $\bar{x}(y)$ and the y -dependent variances $\Delta(y)$ and $\sigma(y)$ obey the following three coupled equations:

$$\bar{x}(y) = Ry + \frac{\eta t}{\alpha} \text{ sgn}(y) \quad \frac{d}{dt}\Delta^2(y) = \frac{2\eta^2 t \sigma^2(y)}{\alpha Q(1-q)} \quad \Delta^2(y) = \sigma^2(y) + B^2 \sigma^4(y)$$

The spin-glass order parameter q is to be solved from the remaining scalar saddle-point equation (6). With help of identities like $\langle x \rangle_* = \bar{x}(y) + zB\sigma^2(y)$, which only hold for conditionally-Gaussian solutions, one can simplify the latter to

$$\frac{\eta^2 t^2}{\alpha} + \alpha \int Dy \Delta^2(y) + (qQ - R^2)(\alpha - 1) = \alpha \left[2 \frac{qQ - R^2}{Q(1-q)} + 1 \right] \int Dy \sigma^2(y)$$

We now immediately find the solution

$$\begin{aligned} \Delta^2(y) &= Q - R^2, & \sigma^2(y) &= Q(1-q), & q &= [\alpha R^2 + \eta^2 t^2]/\alpha Q \\ P[x|y] &= \frac{e^{-\frac{1}{2}[x-Ry-(\eta t/\alpha)\text{ sgn}(y)]^2/(Q-R^2)}}{\sqrt{2\pi(Q-R^2)}} \end{aligned} \quad (26)$$

(this solution is unique). If we calculate the generalization error and the training error from (25) and (26), respectively, we recover the exact expressions

$$E_g = \frac{1}{\pi} \arccos \left[\frac{R_0 + \eta t \sqrt{\frac{2}{\pi}}}{\sqrt{Q_0 + 2\eta t R_0 \sqrt{\frac{2}{\pi}} + \eta^2 t^2 \left[\frac{1}{\alpha} + \frac{2}{\pi} \right]}} \right] \quad (27)$$

$$E_t = \frac{1}{2} - \frac{1}{2} \int Dy \operatorname{erf} \left[\frac{|y| [R_0 + \eta t \sqrt{\frac{2}{\pi}}] + \frac{\eta t}{\alpha}}{\sqrt{2 [Q_0 - R_0^2 + \frac{\eta^2 t^2}{\alpha}]}} \right] \quad (28)$$

Comparison of (25,26) with (20,21) shows that for batch Hebbian learning our theory is fully exact. This is not a big feat as far as Q and R (and thus E_g) are concerned, whose determination did not require knowing the function $\Phi[x, y]$. The fact that our theory also gives the exact values for $P[x|y]$ and E_t , however, is less trivial, since here the disordered nature of the learning dynamics, leading to non-Gaussian distributions, is truly relevant.

3.2 On-Line Hebbian Learning

We next insert the Hebbian recipe $\mathcal{G}[x, y] = \operatorname{sgn}[y]$ into the on-line equations (2,3). Direct analytical solution of these equations, or a demonstration that they are solved by the exact result (18,19), although not ruled out, has not yet been achieved by us. The reason is that here one has conditionally Gaussian field distributions only in special limits. Numerical solution is in principle straightforward, but will be quite CPU intensive (see also a subsequent section). For small learning rates the on-line equations reduce to the batch ones, so we know that in first order in η our on-line equations are exact (for any α, t). We now show that the predictions of our theory are fully exact (i) for Q , R and E_g , (ii) for the first moment (22) of the conditional field distribution, and (iii) for all order parameters in the stationary state. At intermediate times we construct an approximate solution of our equations in order to obtain predictions for $P[x|y]$ and E_t .

As before we choose a Gaussian initial field distribution. Many (but not all) of our previous simplifications still hold, e.g.

$$U = 0, \quad V = \langle x \operatorname{sgn}(y) \rangle, \quad W = \sqrt{2/\pi}, \quad Z = 1$$

(Z did not occur in the batch equations). Thus for on-line learning we find:

$$\frac{d}{dt} Q = 2\eta V + \eta^2 \quad \frac{d}{dt} R = \eta \sqrt{2/\pi}$$

The previous derivation of the identities $\frac{d}{dt} V = \eta/\alpha + 2\eta/\pi$ and $V_0 = R_0 \sqrt{2/\pi}$ still applies (just replace the batch diffusion equation by the on-line one), but the resultant expression for Q is different. Here we obtain:

$$Q = Q_0 + 2\eta t R_0 \sqrt{\frac{2}{\pi}} + \eta^2 t + \eta^2 t^2 \left[\frac{1}{\alpha} + \frac{2}{\pi} \right] \quad R = R_0 + \eta t \sqrt{\frac{2}{\pi}} \quad (29)$$

Comparing (29) with (18) reveals that also for on-line Hebbian learning our theory is exact with regard to Q and R , and thus also with regard to E_g . Upon using $V = \eta t/\alpha + R \sqrt{2/\pi}$, the on-line diffusion equation simplifies to

$$\frac{d}{dt} P[x|y] = \frac{1}{\alpha} \left\{ P[x - \eta \operatorname{sgn}(y)|y] - P[x|y] \right\} - \eta y \sqrt{\frac{2}{\pi}} \frac{\partial}{\partial x} P[x|y] + \frac{1}{2} \eta^2 \frac{\partial^2}{\partial x^2} P[x|y] - \frac{\eta^2 t}{\alpha} \frac{\partial}{\partial x} \left\{ P[x|y] \Phi[x, y] \right\}$$

Multiplication of this equation by x followed by integration over x , together with usage of the general properties $\int dx \{P[x|y]\Phi[x,y]\} = 0$ and $\int dx xP_0[x|y] = R_0y$, gives us the average of the conditional distribution $P[x|y]$ at any time:

$$\bar{x}(y) = \int dx xP[x|y] = Ry + \frac{\eta t}{\alpha} \operatorname{sgn}[y]$$

Comparison with (22) shows also this prediction to be correct.

We now turn to observables which involve more detailed knowledge of the function $\Phi[x,y]$. Our result for $\bar{x}(y)$ and the identity $\langle x \rangle_\star = B^{-1} \frac{\partial}{\partial z} \log \hat{M}[iBz|y]$ allow us to rewrite all remaining equations in Fourier representation, i.e. in terms of $\hat{P}[k|y] = \int dx e^{-ikx} P[x|y]$ and $\hat{M}[k|y] = \int dx e^{-ikx} M[x|y]$:

$$\frac{d}{dt} \log \hat{P}[k|y] = \frac{1}{\alpha} \left[e^{-i\eta k} \operatorname{sgn}(y) - 1 \right] - i\eta ky \sqrt{\frac{2}{\pi}} - \frac{1}{2} \eta^2 k^2 - \frac{i\eta^2 t}{\alpha \hat{P}[k|y] \sqrt{qQ - R^2}} \int Dz z \frac{\hat{M}[k+iBz|y]}{\hat{M}[iBz|y]} \quad (30)$$

with $\log \hat{P}_0[k|y] = -ikR_0y - \frac{1}{2}k^2(Q_0 - R_0^2)$, and with the two saddle-point equations

$$\hat{P}[k|y] = \int Dz \frac{\hat{M}[k+iBz|y]}{\hat{M}[iBz|y]} \quad (31)$$

$$\frac{\eta^2 t^2}{\alpha^2} + \int Dy \int dx P[x|y] [x - \bar{x}(y)]^2 + (1 - \frac{1}{\alpha})(qQ - R^2) = \left[2Q(1 - q) + \frac{1}{B^2} \right] \int Dy Dz \frac{\partial^2}{\partial z^2} \log \hat{M}[iBz|y] \quad (32)$$

Since the fields x grow linearly in time (see our expression for $\bar{x}(y)$) the equations (30,32,31) cannot have proper $t \rightarrow \infty$ limits. To extract asymptotic properties we have to turn to the rescaled distribution $\hat{Q}[k|y] = \hat{P}[k/t|y]$. We define $v(y) = (\eta/\alpha) \operatorname{sgn}(y) + \eta y \sqrt{2/\pi}$. Careful integration of (30), followed by inserting $k \rightarrow k/t$ and by taking the limit $t \rightarrow \infty$, produces:

$$\log \hat{Q}_\infty[k|y] = -ikv(y) - \frac{i\eta^2 k}{\alpha} \int_0^1 du \lim_{t \rightarrow \infty} \frac{t}{\sqrt{qQ - R^2}} \int Dz z \frac{\hat{M}[uk/t + iBz|y]}{\hat{Q}_\infty[uk|y] \hat{M}[iBz|y]} \quad (33)$$

with the functional saddle-point equation

$$\hat{Q}[k|y] = \int Dz \frac{\hat{M}[k/t + iBz|y]}{\hat{M}[iBz|y]} \quad (34)$$

The rescaled asymptotic system (33,34) admits the solution

$$\hat{Q}[k|y] = e^{-ikv(y) - \frac{1}{2}k^2 \tilde{\Delta}^2}, \quad \hat{M}[k|y] = e^{-ik\bar{x}(y) - \frac{1}{2}k^2 \tilde{\sigma}^2 t}$$

with the asymptotic values of B , $\tilde{\Delta}$, $\tilde{\sigma}$ and q determined by solving the following equations:

$$\tilde{\Delta} = B\tilde{\sigma}^2 \quad \tilde{\Delta} = \frac{\eta^2}{\alpha} \lim_{t \rightarrow \infty} \frac{t}{\sqrt{qQ - R^2}} \quad B = \lim_{t \rightarrow \infty} \frac{\sqrt{qQ - R^2}}{Q(1 - q)}$$

$$\eta^2/\alpha^2 + \tilde{\Delta}^2 + (1 - \alpha^{-1}) \lim_{t \rightarrow \infty} (qQ - R^2)/t^2 = 2B^2\tilde{\sigma}^2 \lim_{t \rightarrow \infty} Q(1 - q)/t$$

Inspection shows that these four asymptotic equations are solved by

$$\lim_{t \rightarrow \infty} \tilde{\Delta} = \eta/\sqrt{\alpha}, \quad \lim_{t \rightarrow \infty} q = 1$$

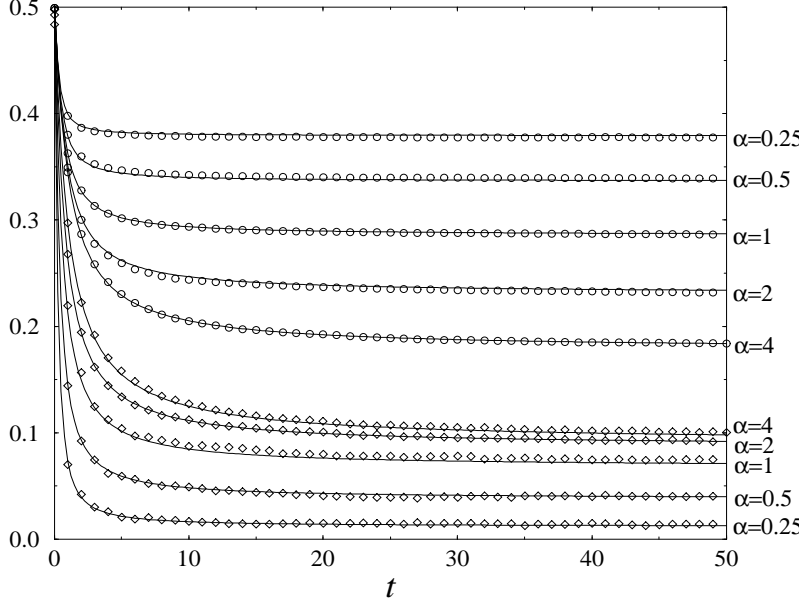


Figure 1: On-line Hebbian learning, simulations versus theoretical predictions, for $\eta = 1$ and $\alpha \in \{0.25, 0.5, 1.0, 2.0, 4.0\}$ ($N = 10,000$). Upper curves: generalization errors as functions of time. Lower curves: training errors as functions of time. Circles: simulation results for E_g ; diamonds: simulation results for E_t . Solid lines: corresponding predictions of dynamical replica theory.

so that

$$\lim_{t \rightarrow \infty} \hat{P}_t[k/t|y] = e^{-ik\eta[\alpha^{-1} \operatorname{sgn}(y) + y\sqrt{2/\pi}] - \frac{1}{2}\eta^2 k^2/\alpha} \quad (35)$$

Comparison with (18,19) shows that this prediction (35) is again exact. Thus the same is true for the asymptotic training error.

Finally, in order to arrive at predictions with respect to $P[x|y]$ and E_t for intermediate times (without rigorous analytical solution of the functional saddle-point equation), and in view of the conditionally-Gaussian form of the field distribution both at $t = 0$ and at $t = \infty$, it would appear to make sense for us to approximate $P[x|y]$ and $M[x|y]$ by simple conditionally Gaussian distributions at any time:

$$P[x|y] = \frac{e^{-\frac{1}{2}[x - \bar{x}(y)]^2/\Delta^2}}{\Delta\sqrt{2\pi}}, \quad M[x|y] = \frac{e^{-\frac{1}{2}[x - \bar{x}(y)]^2/\sigma^2}}{\sigma\sqrt{2\pi}}$$

with the (exact) first moments $\bar{x}(y) = Ry + \eta t \alpha^{-1} \operatorname{sgn}(y)$, and with the variance Δ^2 self-consistently given by the solution of:

$$\begin{aligned} \Delta^2 &= \sigma^2 + B^2 \sigma^4 & B &= \frac{\sqrt{qQ - R^2}}{Q(1-q)} & \frac{d}{dt} \Delta^2 &= \frac{\eta^2}{\alpha} + \eta^2 + \frac{2\eta^2 t \sigma^2}{\alpha Q(1-q)} \\ \alpha \Delta^2 + \frac{\eta^2 t^2}{\alpha} + (qQ - R^2)(\alpha - 1) &= \alpha \sigma^2 \left[2 \frac{qQ - R^2}{Q(1-q)} + 1 \right] \end{aligned}$$

The solution of the above coupled equations behaves as

$$\Delta^2 = Q - R^2 + \eta^2 t/\alpha + \mathcal{O}(t^3) \quad (t \rightarrow 0)$$

$$\Delta^2 = (Q - R^2)[1 + \mathcal{O}(t^{-1})] \quad (t \rightarrow \infty)$$

for short and long times, respectively (note $Q - R^2 \sim t^2$ as $t \rightarrow \infty$). Thus we obtain a simple approximate solution of our equations, which extrapolates between exact results at the temporal boundaries $t = 0$ and $t = \infty$, by putting

$$\Delta^2 = Q - R^2 + \eta^2 t/\alpha$$

with Q and R given by our previous exact result (29), one obtains

$$E_g = \frac{1}{\pi} \arccos \left[\frac{R}{\sqrt{Q}} \right] \quad E_t = \frac{1}{2} - \frac{1}{2} \int Dy \operatorname{erf} \left[\frac{|y|R + \eta t/\alpha}{\Delta \sqrt{2}} \right] \quad (36)$$

We can also calculate the student field distribution $P(x) = \int Dy P[x|y]$, giving

$$P(x) = \frac{e^{-\frac{1}{2}[x + \frac{\eta t}{\alpha}]^2 / (\Delta^2 + R^2)}}{2\sqrt{2\pi(\Delta^2 + R^2)}} \left[1 - \operatorname{erf} \left(\frac{R[x + \frac{\eta t}{\alpha}]}{\Delta \sqrt{2(\Delta^2 + R^2)}} \right) \right] + \frac{e^{-\frac{1}{2}[x - \frac{\eta t}{\alpha}]^2 / (\Delta^2 + R^2)}}{2\sqrt{2\pi(\Delta^2 + R^2)}} \left[1 + \operatorname{erf} \left(\frac{R[x - \frac{\eta t}{\alpha}]}{\Delta \sqrt{2(\Delta^2 + R^2)}} \right) \right] \quad (37)$$

In figure 1 we compare the predictions for the generalization and training errors (36) of the approximate solution of our equations with the results obtained from numerical simulations of on-line Hebbian learning for $N = 10,000$ (initial state: $Q_0 = 1$, $R_0 = 0$; learning rate: $\eta = 1$). All curves show excellent agreement between theory and experiment. For E_g this is guaranteed by the exactness of our theory for Q and R ; the agreement found for E_t is more surprising, in that these predictions are obtained from a simple approximation of the solution of our equations. We also compare the theoretical predictions made for the distribution $P[x|y]$ with the results of numerical simulations. This is done in figure 2, where we show the fields as observed at time $t = 50$ in simulations ($N = 10,000$, $\eta = 1$, $R_0 = 0$, $Q_0 = 1$) of on-line Hebbian learning, for three different values of α . In the same figure we draw (as dashed lines) the theoretical prediction (22) for the y -dependent average of the conditional x -distribution $P[x|y]$. Finally we compare the student field distribution $P(x)$, as observed in simulations of on-line Hebbian learning ($N = 10,000$, $\eta = 1$, $R_0 = 0$, $Q_0 = 1$) with our prediction (37). The result is shown in figure 3, for $\alpha \in \{4, 1, 0.25\}$. In all cases the agreement between theory and experiment, even for the approximate solution of our equations, is quite satisfactory.

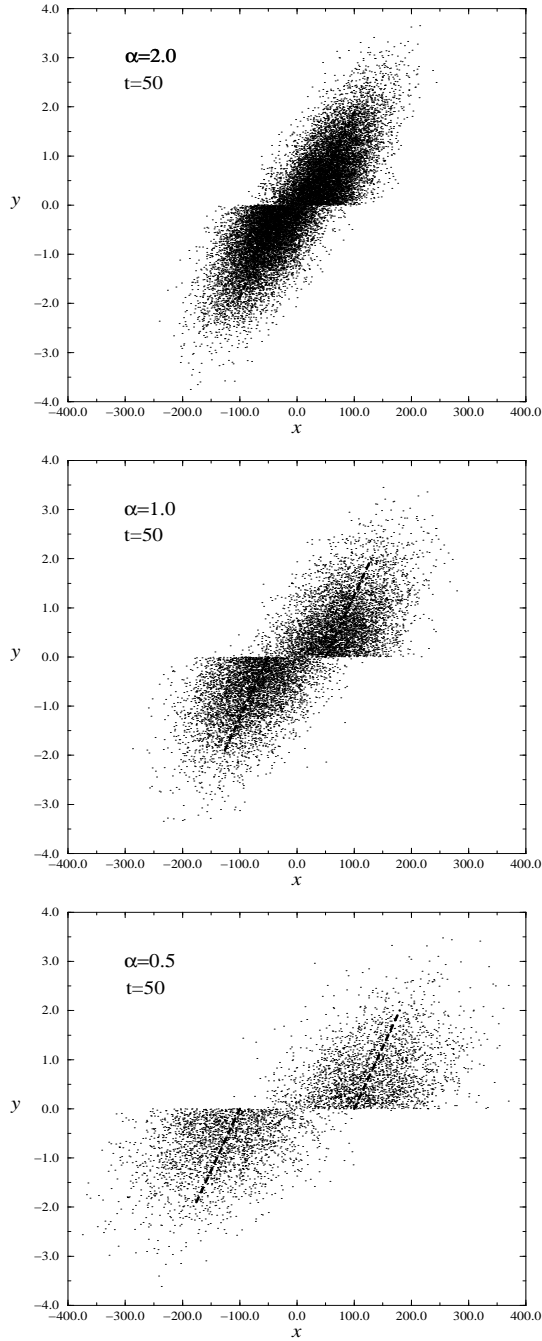


Figure 2: Comparison between simulation results for on-line Hebbian learning (system size $N = 10,000$) and dynamical replica theory, for $\eta = 1$ and $\alpha \in \{0.5, 1.0, 2.0\}$. Dots: local fields $(x, y) = (\mathbf{J} \cdot \boldsymbol{\xi}, \mathbf{B} \cdot \boldsymbol{\xi})$ (calculated for questions in the training set), at time $t = 50$. Dashed lines: conditional average of student field x as a function of y , as predicted by the theory, $\bar{x}(y) = Ry + (\eta t / \alpha) \operatorname{sgn}(y)$.

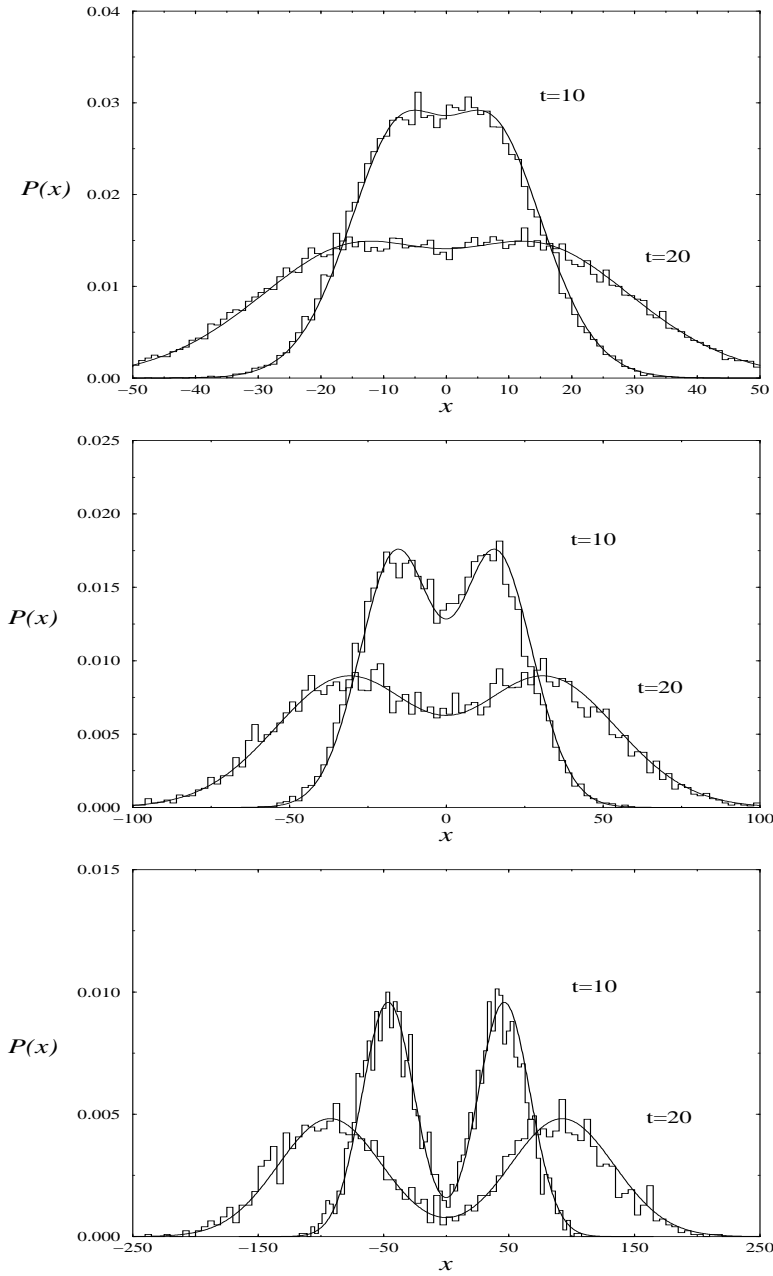


Figure 3: Simulations of on-line Hebbian learning with $\eta = 1$ and $N = 10,000$. Histograms: student field distributions measured at $t = 10$ and $t = 20$. Lines: theoretical predictions for student field distributions. $\alpha = 4$ (upper), $\alpha = 1$ (middle), $\alpha = 0.25$ (lower).

4 General Approximation Schemes

All three approximation schemes presented in this section aim at providing alternatives to calculating the effective measure $M[x|y]$ at each time step from the functional saddle-point equation. Since this calculation cannot (yet) be done analytically, it constitutes a significant numerical obstacle in working out the predictions of our theory. Each scheme preserves both normalisation and symmetries of the probability density $P[x, y]$ and its marginals, as well as the relation $\int dx P[x|y]\Phi[x, y] = 0$ for all y . In the first two approximation schemes, a large α expansion and a conditionally-Gaussian saddle-point approximation, all Gaussian integrals representing the disorder in the problem can be done analytically; this leads to a significant reduction in CPU time when solving our equations numerically (especially the large α approximation is extremely simple and fast, as it does not even involve a saddle-point equation for q). We only work out the equations for on-line learning; the batch laws follows as usual upon expanding the equations in powers of η and retaining only the linear terms.

4.1 Large α Approximation

Our first approximation scheme is obtained upon taking into account the finite nature of the training set (i.e. the disordered nature of the dynamics) in first non-trivial order. The amount of disorder is effectively measured by the parameter B , or, equivalently, by the deviation of the value of the spin-glass order parameter q from its naive value R^2/Q . Putting $B = 0$ in the saddle-point equation (7) immediately gives $\lim_{B \rightarrow 0} M[x|y] = P[x|y]$, so we write

$$M[x|y] = P[x|y] \left[1 + \sum_{\ell > 0} B^\ell m_\ell[x|y] \right], \quad \int dx P[x|y] m_\ell[x|y] = 0 \quad (38)$$

Upon inserting (38) as an *ansatz* into the saddle-point equation (7), one easily shows that

$$M[x|y] = P[x|y] e^{-\frac{1}{2}B^2[x - \bar{x}(y)]^2 + \frac{1}{2}B^2[\bar{x}^2(y) - \bar{x}(y)^2] + \mathcal{O}(B^3)} \quad (39)$$

with the abbreviations

$$\bar{x}(y) = \int dx P[x|y]x \quad \bar{x}^2(y) = \int dx P[x|y]x^2$$

(the second $\mathcal{O}(B^2)$ term in the exponent of (39), being independent of x , just reflects the normalisation requirements). This result enables us, in turn, to expand the function $\Phi[x, y]$ which controls the non-trivial term in our diffusion equation for $P[x|y]$. Note that from the definition of B it follows that $Q(1-q) = \frac{1}{2}B^{-2}[\sqrt{1+4B^2(Q-R^2)}-1]$, which gives

$$\Phi[x, y] = \frac{x - \bar{x}(y)}{Q - R^2} + \mathcal{O}(B^2)$$

With this expression we can write our approximate equations in explicitly closed form (i.e. without any remaining saddle-point equations). The relevant scalar functions become

$$U = \frac{\langle \mathcal{G}[x, y][x - \bar{x}(y)] \rangle}{Q - R^2} \quad V = \langle x\mathcal{G}[x, y] \rangle \quad W = \langle y\mathcal{G}[x, y] \rangle \quad Z = \langle \mathcal{G}^2[x, y] \rangle \quad (40)$$

For on-line learning we find:

$$\frac{d}{dt}Q = 2\eta V + \eta^2 Z \quad \frac{d}{dt}R = \eta W \quad (41)$$

$$\begin{aligned} \frac{d}{dt} P[x|y] &= \frac{1}{\alpha} \int dx' P[x'|y] [\delta[x-x'-\eta\mathcal{G}[x',y]] - \delta[x-x']] - \eta \frac{\partial}{\partial x} \left\{ P[x|y] [U(x-Ry) + Wy] \right\} \\ &\quad + \frac{1}{2} \eta^2 Z \frac{\partial^2}{\partial x^2} P[x|y] - \eta \left[\frac{V-RW}{Q-R^2} - U \right] \frac{\partial}{\partial x} \left\{ P[x|y] [x - \bar{x}(y)] \right\} \end{aligned} \quad (42)$$

From the solution of the above equations follow, as always, the training- and generalization errors $E_t = \int Dydx P[x|y]\theta[-xy]$ and $E_g = \pi^{-1} \arccos[R/\sqrt{Q}]$. The resulting theory is obviously exact in the limit $\alpha \rightarrow \infty$ (see [1]), by construction.

4.2 Conditionally-Gaussian Approximation

Our basic idea here is a variational approach to solving the functional saddle-point problem (valid for any α), i.e. to carry out the functional extremisation only within the restricted family of conditionally Gaussian measures $M[x|y]$ (which, together with q , characterises the saddle-point):

$$M[x|y] = \frac{e^{-\frac{1}{2}[x-\bar{x}(y)]^2/\sigma^2(y)}}{\sigma(y)\sqrt{2\pi}}$$

Note that this does not imply the stronger statement that $P[x|y]$ itself is taken to be of a conditionally-Gaussian form (as in the case of the approximation used for on-line Hebbian learning). Extremisation of the original replica-symmetric functional $\Psi[q, \{M\}]$ (see [1]) within the conditionally-Gaussian family of functions results in the requirement that the two y -dependent moments $\bar{x}(y)$ and $\sigma^2(y)$ be given by

$$\bar{x}(y) = \int dx x P[x|y], \quad \Delta^2(y) = \int dx x^2 P[x|y] - \bar{x}^2(y) = \sigma^2(y) + B^2 \sigma^4(y)$$

Now we can again calculate all relevant averages which involve the effective measure $M[x|y]$ exactly. In particular:

$$\langle x \rangle_\star = \bar{x}(y) + zB\sigma^2(y) \quad B = \frac{\sqrt{qQ-R^2}}{Q(1-q)} \quad \Phi[x, y] = \frac{e^{-\frac{1}{2}[x-\bar{x}(y)]^2/\Delta^2(y)}}{\Delta(y)\sqrt{2\pi}P[x|y]} \frac{(x-\bar{x}(y))\sigma^2(y)}{Q(1-q)\Delta^2(y)}$$

For on-line learning this results in the following approximated theory:

$$U = \int DyDu \left\{ \frac{u\sigma^2(y)\mathcal{G}[\bar{x}(y) + u\Delta(y), y]}{Q(1-q)\Delta(y)} \right\}$$

$$V = \langle x\mathcal{G}[x, y] \rangle \quad W = \langle y\mathcal{G}[x, y] \rangle \quad Z = \langle \mathcal{G}^2[x, y] \rangle \quad (43)$$

$$\frac{d}{dt} Q = 2\eta V + \eta^2 Z \quad \frac{d}{dt} R = \eta W \quad (44)$$

$$\begin{aligned} \frac{d}{dt} P[x|y] &= \frac{1}{\alpha} \int dx' P[x'|y] [\delta[x-x'-\eta\mathcal{G}[x',y]] - \delta[x-x']] - \eta \frac{\partial}{\partial x} \left\{ P[x|y] [U(x-Ry) + Wy] \right\} \\ &\quad + \frac{1}{2} \eta^2 Z \frac{\partial^2}{\partial x^2} P[x|y] - \frac{\eta\sigma^2(y) [V-RW-(Q-R^2)U]}{\sqrt{2\pi}Q(1-q)\Delta^5(y)} [\Delta^2(y) - (x-\bar{x}(y))^2] e^{-\frac{1}{2}[x-\bar{x}(y)]^2/\Delta^2(y)} \end{aligned} \quad (45)$$

The remaining order parameter q is calculated at each time-step by solving

$$\langle (x-Ry)^2 \rangle + (qQ-R^2)(1-\frac{1}{\alpha}) = \left[2\frac{qQ-R^2}{Q(1-q)} + 1 \right] \int Dy \sigma^2(y)$$

From the solution of these equations follow the training- and generalization errors $E_t = \int Dydx P[x|y]\theta[-xy]$ and $E_g = \pi^{-1} \arccos[R/\sqrt{Q}]$.

4.3 Partially Annealed Approximation

In order to construct our third and final approximation we return to an earlier stage of the derivation of the present formalism (see [1]), and rewrite the functional saddle-point equation in a form where the replica limit $n \rightarrow 0$ has not yet been taken, i.e.

$$\text{for all } x, y : \quad P[x|y] = \frac{\int Dz \, M_n[x|y] e^{Bz[x-\bar{x}(y)]} \left[\int dx' \, M_n[x'|y] e^{Bz[x'-\bar{x}(y)]} \right]^{n-1}}{\int Dz \left[\int dx' \, M_n[x'|y] e^{Bz[x'-\bar{x}(y)]} \right]^n}$$

with $\bar{x}(y) = \int dx \, x P[x|y]$. In our full (quenched disorder) calculation we find ourselves with the effective measure $M[x|y] = \lim_{n \rightarrow 0} M_n[x|y]$. In contrast, an alternative calculation, whereby the quenched average over all training sets would have been replaced by an annealed average over all training sets, would have led us to the value $n = 1$ rather than $n = 0$: $M[x|y] = M_1[x|y]$. We can now define in a natural way an annealed approximation of our theory upon replacing the complicated $n = 0$ functional saddle-point equation (7) by the much simpler $n = 1$ version:

$$P[x|y] = \frac{\int Dz \, M[x|y] e^{Bz[x-\bar{x}(y)]}}{\int Dz \int dx' \, M[x'|y] e^{Bz[x'-\bar{x}(y)]}}$$

The z -integrations can immediately be carried out, and the resulting equation solved for $M[x|y]$, giving:

$$M[x|y] = \frac{P[x|y] e^{-\frac{1}{2}B^2[x-\bar{x}(y)]^2}}{\int dx' \, P[x'|y] e^{-\frac{1}{2}B^2[x'-\bar{x}(y)]^2}}, \quad (46)$$

Averages involving the effective measure $M[x|y]$ are thus written explicitly in terms of $P[x|y]$, and we are left with the following approximate theory:

$$U = \langle \Phi[x, y] \mathcal{G}[x, y] \rangle \quad V = \langle x \mathcal{G}[x, y] \rangle \quad W = \langle y \mathcal{G}[x, y] \rangle \quad Z = \langle \mathcal{G}^2[x, y] \rangle \quad (47)$$

$$\frac{d}{dt} Q = 2\eta V + \eta^2 Z \quad \frac{d}{dt} R = \eta W \quad (48)$$

$$\begin{aligned} \frac{d}{dt} P[x|y] &= \frac{1}{\alpha} \int dx' P[x'|y] [\delta[x-x'-\eta \mathcal{G}[x', y]] - \delta[x-x']] - \eta \frac{\partial}{\partial x} \left\{ P[x|y] [U(x-Ry) + Wy] \right\} \\ &\quad + \frac{1}{2} \eta^2 Z \frac{\partial^2}{\partial x^2} P[x|y] - \eta \left[V - RW - (Q - R^2)U \right] \frac{\partial}{\partial x} \left\{ P[x|y] \Phi[x, y] \right\} \end{aligned} \quad (49)$$

with

$$\Phi[X, y] = \frac{1}{Q(1-q)} \int Dz \left\{ \frac{\int dx \, P[x|y] e^{-\frac{1}{2}[B(x-\bar{x}(y))-z]^2} e^{-\frac{1}{2}[B(X-\bar{x}(y))-z]^2} (X-x)}{\left[\int dx \, P[x|y] e^{-\frac{1}{2}[B(x-\bar{x}(y))-z]^2} \right]^2} \right\}$$

As always, $B = \sqrt{qQ-R^2}/Q(1-q)$. The remaining spin-glass order parameter q is calculated at each time-step by solving

$$\langle (x-Ry)^2 \rangle + (qQ-R^2)(1-\frac{1}{\alpha}) = \left[2(qQ-R^2)^{\frac{1}{2}} + \frac{1}{B} \right] \int Dy Dz \, z \left\{ \frac{\int dx \, P[x|y] e^{-\frac{1}{2}[B(x-\bar{x}(y))-z]^2} x}{\int dx \, P[x|y] e^{-\frac{1}{2}[B(x-\bar{x}(y))-z]^2}} \right\}$$

From the solution of the above equations follow the training- and generalization errors $E_t = \langle \theta[-xy] \rangle$ and $E_g = \pi^{-1} \arccos[R/\sqrt{Q}]$. It should be emphasised that the present approximation is not equivalent to (and should be more accurate than) a full annealed treatment of the disorder in the problem; the latter would have affected not only the equation for $M[x|y]$ but also the saddle-point equation for q (hence the name *partially* annealed approximation).

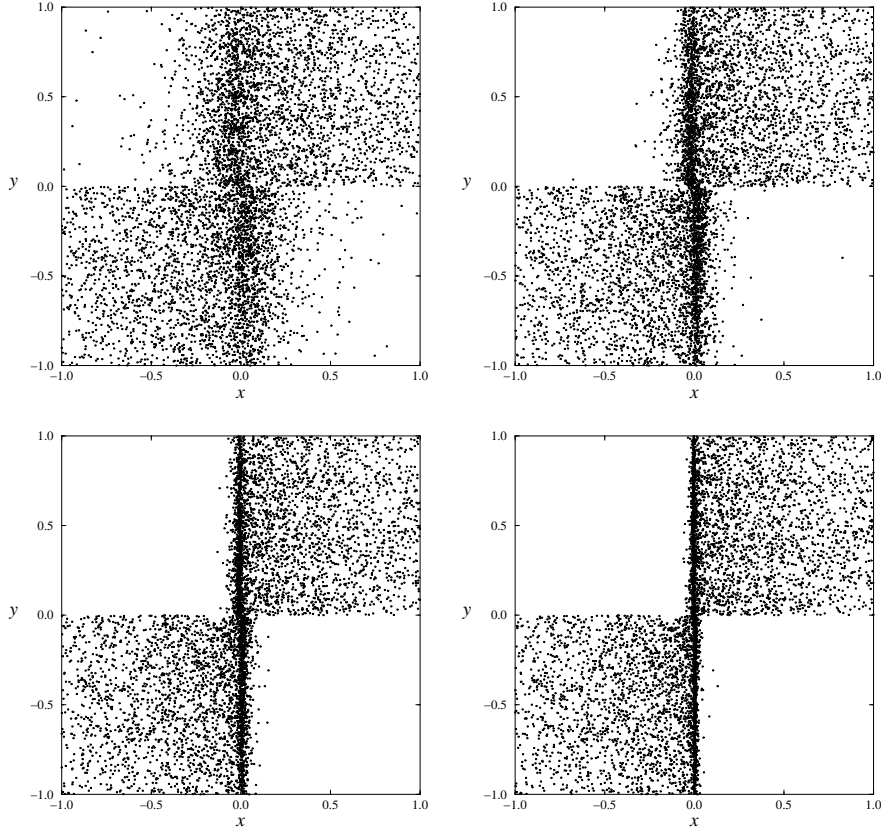


Figure 4: Numerical simulations of on-line Adatron learning, with $N=10,000$, $\alpha=1$ and $\eta=\frac{1}{2}$. The scatter plots show the observed student and teacher fields $(x, y) = (\mathbf{J} \cdot \boldsymbol{\xi}, \mathbf{B} \cdot \boldsymbol{\xi})$ at times $t=5$ (upper left), $t=10$ (upper right), $t=15$ (lower left) and $t=20$ (lower right), as measured during simulations for the data in the training set \tilde{D} , drawn as points in the (x, y) plane. Note the development over time of an increasingly narrow ‘ridge’ along the line $x=0$.

5 Non-Hebbian Rules: Theory versus Simulations

Henceforth we will always assume initial states with specified values for R_0 and Q_0 but without correlations with the training set, i.e.

$$P_0[x|y] = \frac{e^{-\frac{1}{2}[x-R_0y]^2/(Q_0-R_0^2)}}{\sqrt{2\pi(Q_0-R_0^2)}}$$

This implies that the student could initially have some knowledge of the rule to be learned, if we wish, but will never know beforehand about the composition of the training set. We will inspect the learning dynamics generated upon using two of the most common non-Hebbian (error-correcting) learning rules:

$$\begin{aligned} \text{Perceptron : } \quad \mathcal{G}[x, y] &= \text{sgn}(y)\theta[-xy] \\ \text{AdaTron : } \quad \mathcal{G}[x, y] &= |x| \text{sgn}(y)\theta[-xy] \end{aligned} \tag{50}$$

Note that in the case of AdaTron learning the cases $\eta \leq 1$ and $\eta > 1$ give rise to qualitatively different behaviour of the first term in the diffusion equation (3). For $\eta < 1$ the learning process, aiming at the situation where $xy > 0$ never occurs, remedies inappropriate student fields by slowly moving them towards (but not immediately across) the decision boundary. For $\eta > 1$ the adjustments made to the student fields could move them well into the region at the other side of the decision boundary. The case $\eta = 1$ is special, in that changes to the student fields tend to move them precisely onto the decision boundary. The student field distribution consequently develops a δ -peak at the origin, in perfect agreement with what can be observed in numerical simulations (see e.g. the figures referring to on-line AdaTron learning with $\eta = 1$ in [1]):

$$\eta = 1 : \quad \frac{d}{dt} P[x|y] = \frac{1}{\alpha} \left\{ \delta(x) \int dx' \theta[-x'y] P[x'|y] - P[x|y] \theta[-xy] \right\} + \dots$$

In fact the same occurs for all $\eta \leq 1$: about half of the probability weight of $P[x|y]$ will in due course become concentrated in an increasingly thin ridge along the decision boundary $x = 0$. This is illustrated in figure 4, for $\eta = \frac{1}{2}$. Since such a singular behaviour (although in principle accurately described by our equations) will be difficult to reproduce when solving the equations numerically, using finite spatial resolution, we will in this paper only deal with the case of $\eta > 1$ for AdaTron learning.

5.1 Large α and Conditionally-Gaussian Approximations

Our first approximated theory (the large α approximation) is very simple, with neither saddle-point equations to be solved nor nested integrations. As a result, numerical solution of the macroscopic equations is straightforward and fast. In figures 5 (on-line perceptron learning) and 6 (on-line Adatron learning) we compare the results of solving the coupled equations (40,41,42) numerically for finite values of α , plotting the generalisation- and training errors as functions of time, with results obtained from performing numerical simulations. As could have been expected, the large α approximation under-estimates the amount of disorder in the learning process, which immediately translates into under-estimation of the gap between E_t and E_g (which is its fingerprint). It is also clear from these figures that, although at any given time the quality of the predictions of this approximation does improve when α increases (as indeed it should), and although there is surely qualitative agreement, reliably accurate quantitative statements on the values of the training- and generalisation errors are confined to the regime $\eta t \leq \alpha$. Yet, surprisingly, the agreement obtained is very good, even for $\eta t > \alpha$. Apparently the present approximation does still capture the main characteristics of the (non-Gaussian) joint field distribution. This is illustrated quite clearly and explicitly in figures 7 and 8, where we compare for a fixed time $t = 10$ the student and teacher fields as measured during numerical simulations (for $N = 10,000$, drawn as dots in the (x, y) plane) for the $p = \alpha N$ questions ξ^μ in the training set \tilde{D} , to the theoretical predictions for the joint field distribution $P[x, y]$ (drawn as contour plots). We will not at this stage attempt to explain the surprising effectiveness of the large α approximation for small values of α (note that figures 5 and 6 even suggest an increase in accurateness as α is lowered below $\alpha = 1$). This would require a systematic mathematical analysis of the non-linear diffusion equation (42), which we consider to be beyond the scope of the present paper.

The conditionally-Gaussian approximation again involves no nested integrals, and its equations can therefore still be solved numerically in a reasonably fast way, but it does already require the solution (at each infinitesimal time step) of a scalar saddle-point equation to determine the spin-glass order parameter q . Approximations of this type work extremely well for the simple Hebbian learning

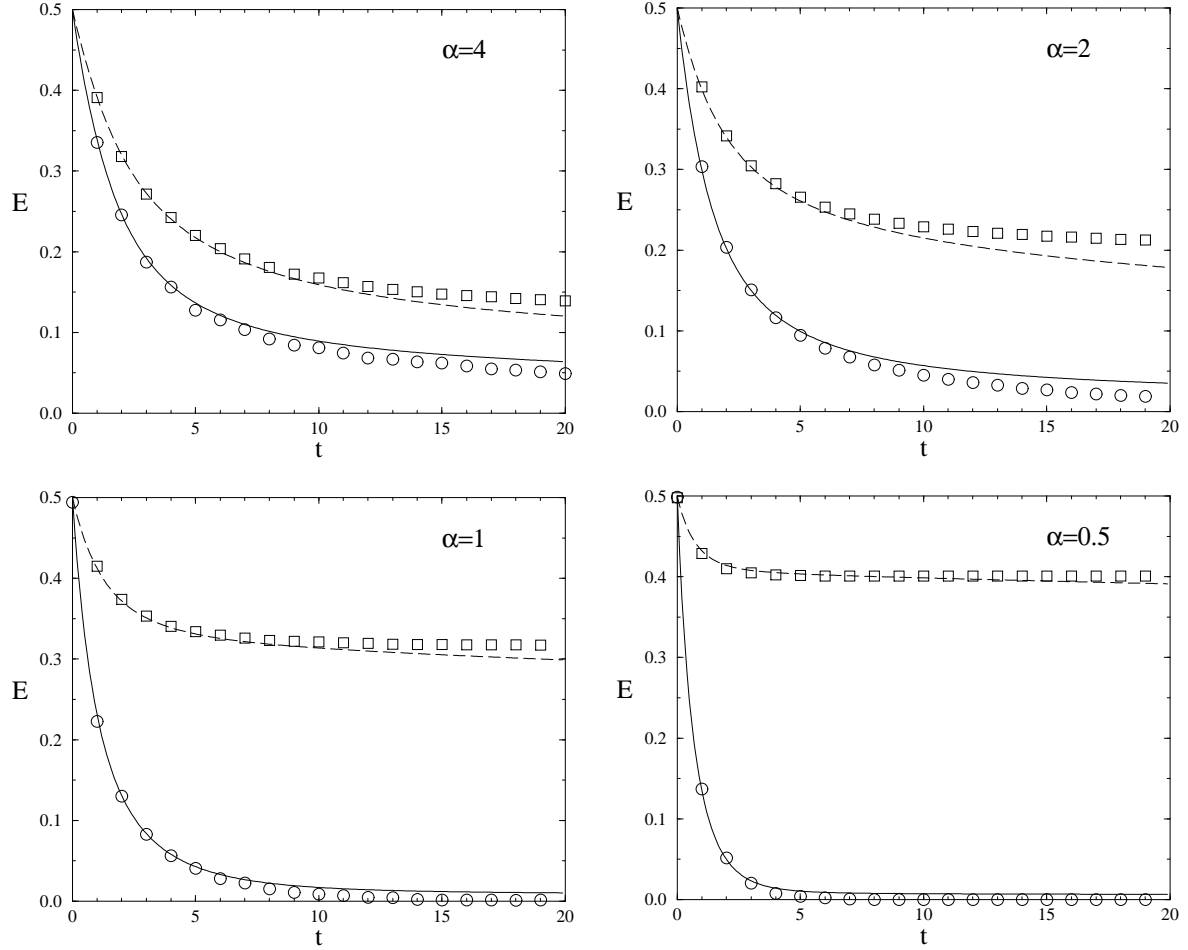


Figure 5: Comparison between the large α approximation of the theory and numerical simulations of on-line perceptron learning with $N = 10,000$ and $\eta = 1$. Markers: training errors E_t (circles) and generalisation errors E_g (squares); finite size effects in the simulation data are of the order of the marker size. Lines: theoretical predictions for training errors (solid) and generalisation errors (dashed) as functions of time, according to the approximated theory. Training set sizes: $\alpha = 4$ (upper left), $\alpha = 2$ (upper right), $\alpha = 1$ (lower left), and $\alpha = 0.5$ (lower right).

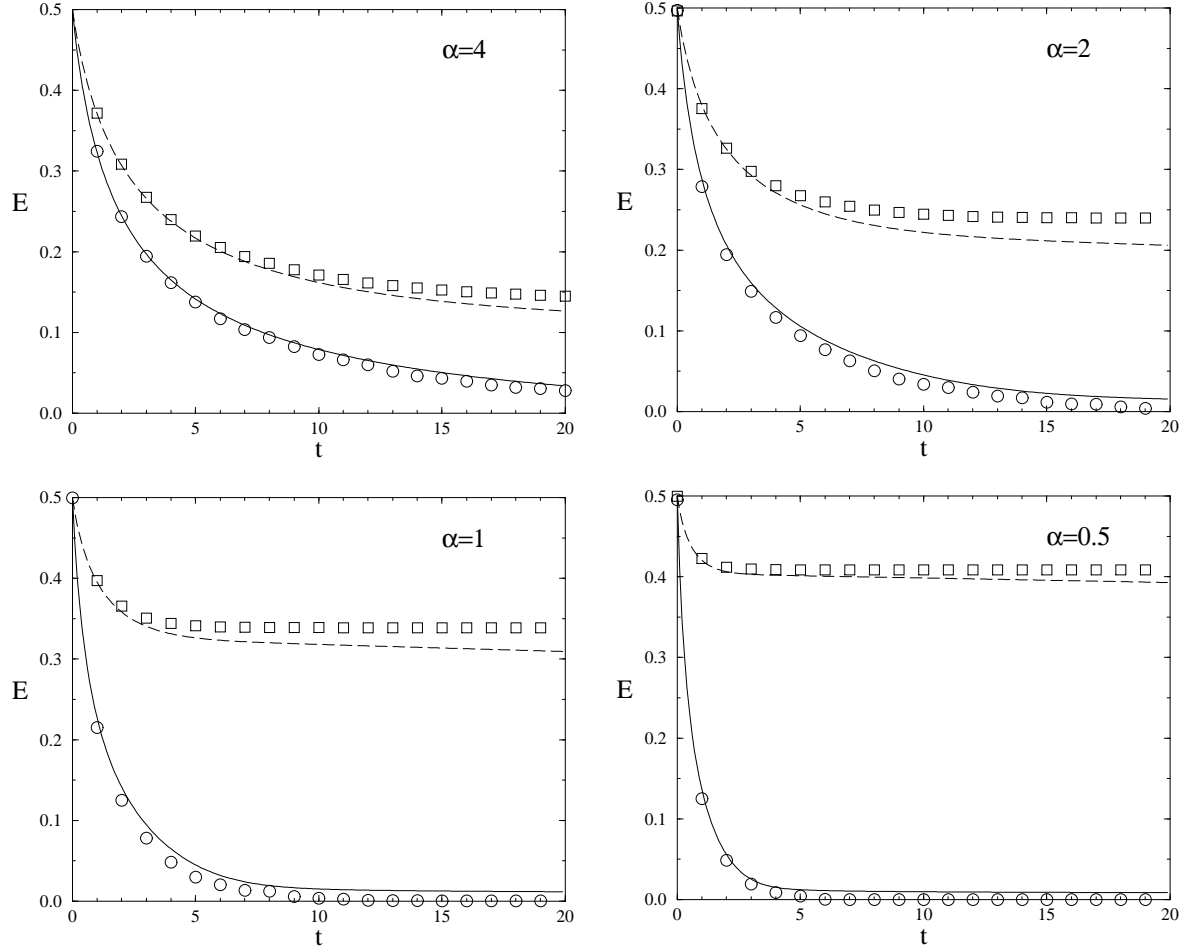


Figure 6: Comparison between the large α approximation of the theory and numerical simulations of on-line Adatron learning with $N = 10,000$ and $\eta = 2$. Markers: training errors E_t (circles) and generalisation errors E_g (squares); finite size effects in the simulation data are of the order of the marker size. Lines: theoretical predictions for training errors (solid) and generalisation errors (dashed) as functions of time, according to the approximated theory. Training set sizes: $\alpha = 4$ (upper left), $\alpha = 2$ (upper right), $\alpha = 1$ (lower left), and $\alpha = 0.5$ (lower right).

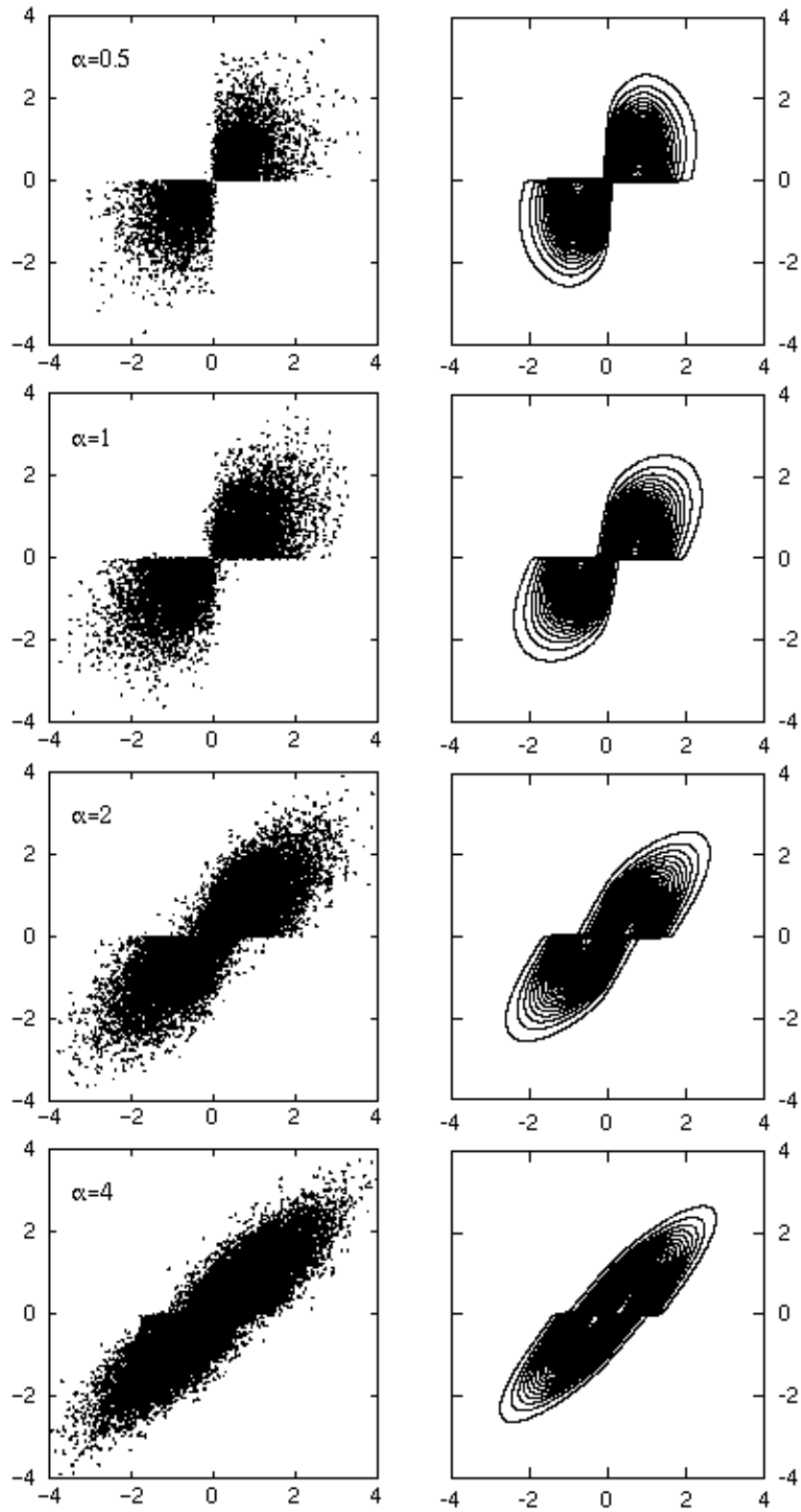


Figure 7: Comparison between the large α approximation of the theory and numerical simulations of on-line Perceptron learning, with $N = 10,000$ and $\eta = 1$. Scatter plots (left): observed student and teacher fields $(x, y) = (\mathbf{J} \cdot \boldsymbol{\xi}, \mathbf{B} \cdot \boldsymbol{\xi})$ as measured at time $t = 10$ during simulations, for the data in \tilde{D} , drawn in the (x, y) plane. Contour plots (right): corresponding predictions for the joint field distribution $P[x, y]$, according to the approximated theory. Training set sizes: $\alpha = 0.5, 1, 2, 4$ (from top to bottom).

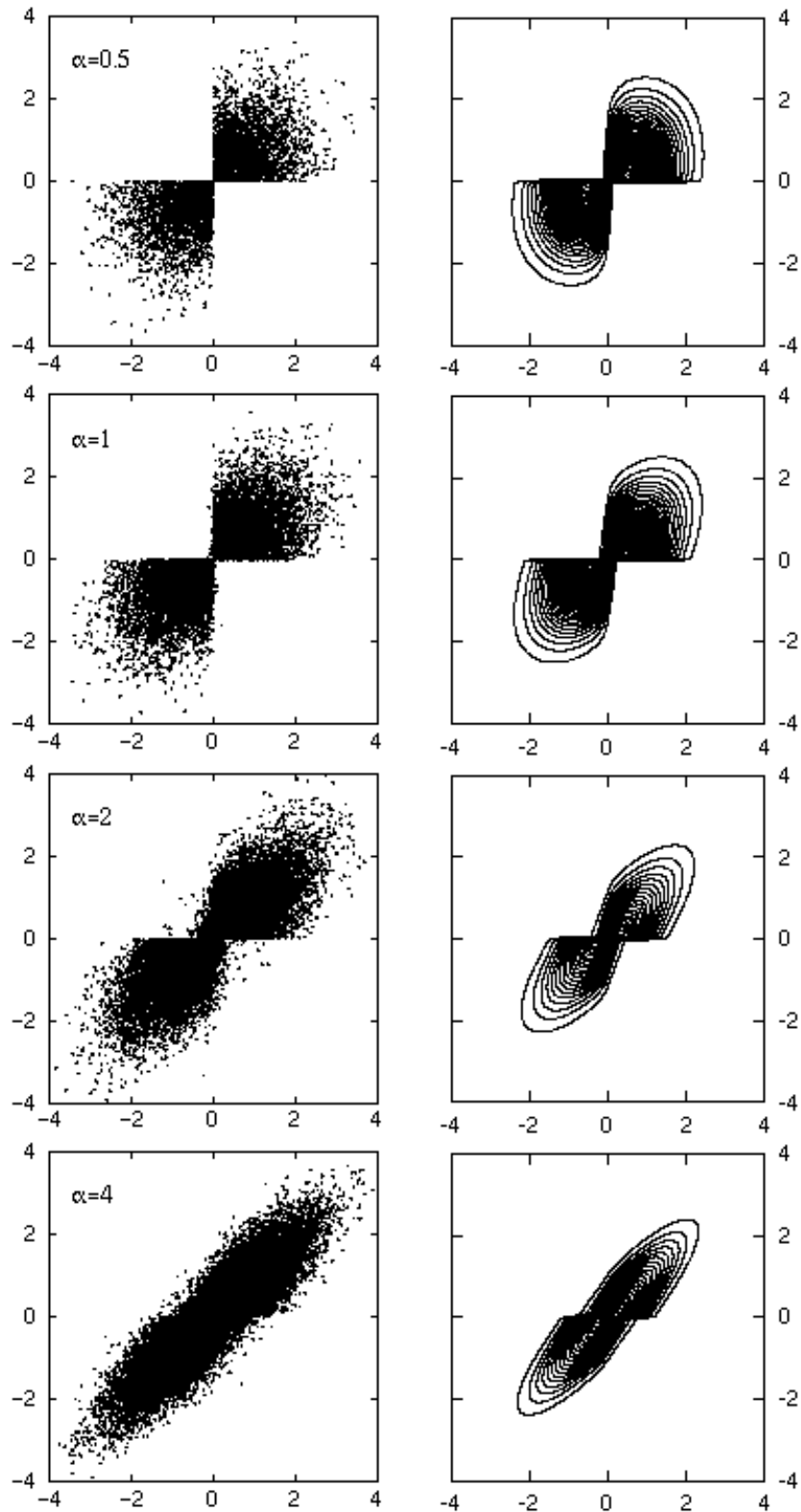


Figure 8: Comparison between the large α approximation of the theory and numerical simulations of on-line Adatron learning with $N = 10,000$ and $\eta = 2$. Scatter plots (left): observed student and teacher fields $(x, y) = (J \cdot \xi, B \cdot \xi)$ as measured at time $t = 10$ during simulations, for the data in \tilde{D} , drawn in the (x, y) plane. Contour plots (right): corresponding predictions for the joint field distribution $P[x, y]$, according to the approximated theory. Training set sizes: $\alpha = 0.5, 1, 2, 4$ (from top to bottom).

rules, as we have seen earlier. However, numerical solution of the coupled equations (43,44,45) shows quite clearly that for the more sophisticated non-Hebbian rules such as Perceptron and AdaTron, which are of an error correcting nature (i.e. where changes are made only when student and teacher disagree), the conditionally-Gaussian approximation is less accurate than the previously investigated large α approximation, in spite of the fact that the latter involved much simpler equations. Apparently the generally non-Gaussian nature of the conditional distribution $P[x|y]$, and thereby of the measure $M[x|y]$, is of crucial importance. It is not good enough to try getting away with allowing the y -dependent averages $\bar{x}(y)$ and variances $\Delta(y)$ to be non-trivial functions. With conditionally-Gaussian measures $M[x|y]$ it turns out that generating the right width of the conditional distributions $P[x|y]$ inevitably introduces tails for $P[x|y]$ which spill into the $xy < 0$ region, which are found to be absent in error-correcting learning rules such as Perceptron and Adatron. This picture is consistent with figures 7 and 8, where we can observe that for any fixed value of the teacher field y the remaining marginal distribution for x is generally not symmetric around its (y -dependent) average. We conclude that the conditionally-Gaussian approximation is generally inferior to the large α approximation. We will not waste paper by producing large numbers of graphs to illustrate this explicitly and comprehensively, but we will rather draw the conditionally-Gaussian predictions together with those of the other approximations and of the full theory, by way of illustration.

5.2 Partially Annealed Approximation and Full Equations

The partially annealed approximation and the full theory are both expected to improve upon the large α approximation (note that the partially annealed approximation can be seen as an improved version of the large α approximation, similar in structure but valid also for small α , i.e. large B). Although the partially annealed approximation does not involve a functional saddle-point equation to be solved (which improves numerical speed), it shares with the full theory the appearance of nested (Gaussian) integrals, namely those appearing in the function $\Phi[x, y]$ and in the saddle-point equation for q . Thus, solution of both the full theory and of the partially annealed approximation involves a significant amount of CPU time (avoiding standard instabilities of discretised diffusion equations sets further limits on the maximum size of the time discretisation, dependent on the field resolution [8]), which implies that we have to reduce our ambition and restrict the number of experiments to a few typical ones.

We will thus investigate two examples, both with $\alpha = 1$: on-line Perceptron learning with $\eta = \frac{1}{2}$, and on-line AdaTron learning with $\eta = \frac{3}{2}$. We solve numerically the full equations of our theory, i.e. the macroscopic dynamical laws (2,3) with the order parameters calculated at each time step by solving (6,7), and show in figure 9 the training and generalisation errors as functions of time together with the corresponding values as measured during numerical simulations, with systems of size $N = 10,000$. In addition, we plot in the same picture, for comparison, the training- and generalisation errors obtained by numerical solution of the three approximated theories as derived in the previous section. In comparing curves we have to take into account that those describing the large α approximation were generated upon solving the diffusion equation with a significantly higher numerical field resolution ($\Delta x = 0.015$) than the others (where we used $\Delta x = 0.05$), because of CPU limitations. A restricted field resolution is likely to be more critical at large times, where the probability weight in the $xy < 0$ region, responsible for the residual error and for the non-stationarity of the dynamics, is highly concentrated close to the decision boundary $x = 0$. Especially for large times, we should therefore expect the full theory, the conditionally-Gaussian approximation, and the partially annealed approximation to all three perform better in reality than what is suggested by the numerical solutions

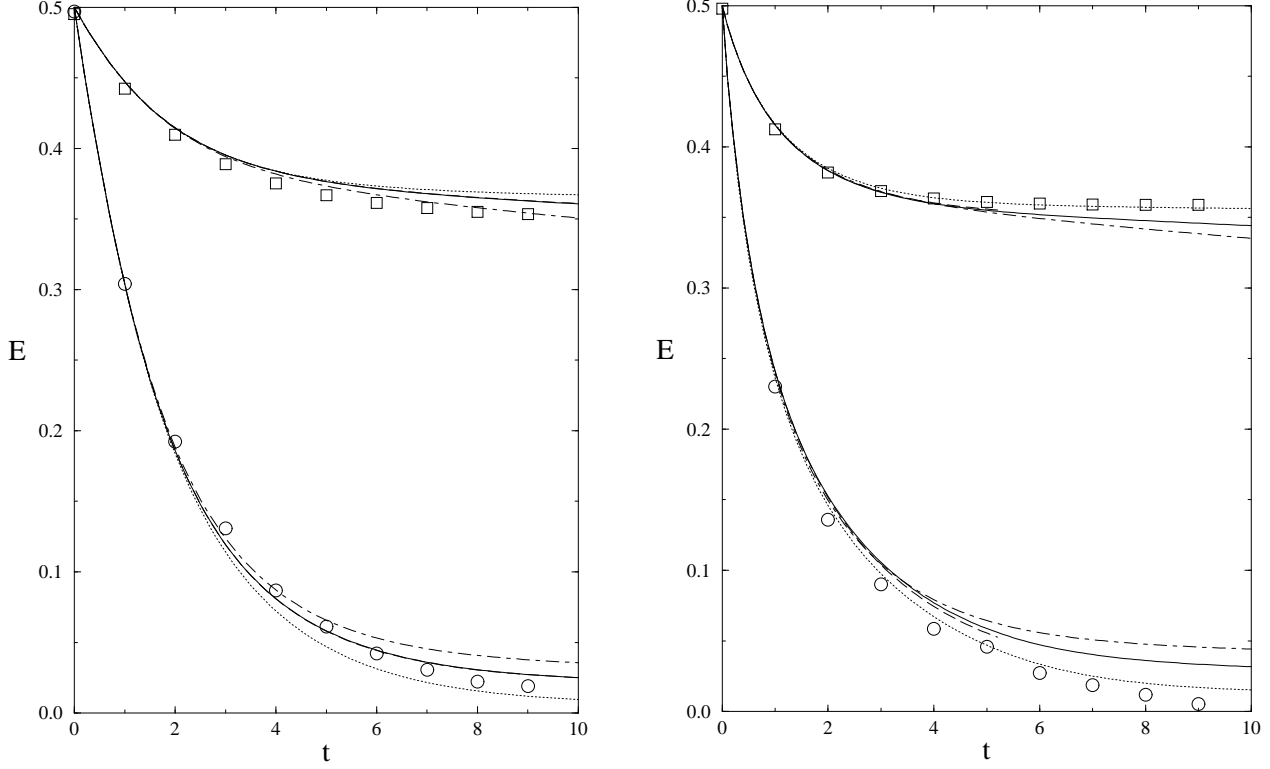


Figure 9: Comparison between the full numerical solution of our equations, as well as the three approximations of the theory, and the results of doing numerical simulations of on-line learning with $N = 10,000$ and $\alpha = 1$. Markers: training errors E_t (circles) and generalisation errors E_g (squares); finite size effects are of the order of the size of the markers. Lines: theoretical predictions for training errors (lower) and generalisation errors (upper) as functions of time, according to the theory. The different line types refer to: full equations (solid), annealed approximation (dashed), conditionally-Gaussian approximation (dashed-dotted) and large α approximation (dotted) (note: the dashed and solid curves fall virtually on top of one another). Left picture: Perceptron learning, with $\eta = \frac{1}{2}$. Right picture: AdaTron learning, with $\eta = \frac{3}{2}$.

of their equations as shown in figure 9. This is particularly true for AdaTron learning, where even for $\eta > 1$ (where we do not expect to observe a δ -singularity) the field distributions still tend to develop a jump discontinuity at $x = 0$. It turns out that the curves of the full theory and those of the partially annealed approximation are very close (virtually on top of one another for the case of Perceptron learning) in figure 9; apparently for the learning times considered here there is no real need to evaluate the full theory.

Finally, we show in figure 10 for both the full theory and for the simulation experiments the two distributions $P^\pm(x) = \int dy P[x, y]\theta[\pm y]$ for the student fields, given a specified sign of the teacher field y (and thus a given teacher output), corresponding to the same experiments. Note that $P(x) = P^+(x) + P^-(x)$. The pictures in figure 10 again illustrate quite clearly the difference between learning with restricted training sets and learning with infinite training sets: in the former case the desired agreement $xy > 0$ between student and teacher is achieved by a qualitative *deformation* of $P[x|y]$, away from the initial Gaussian shape, rather than by adaptation of the first and second order moments.

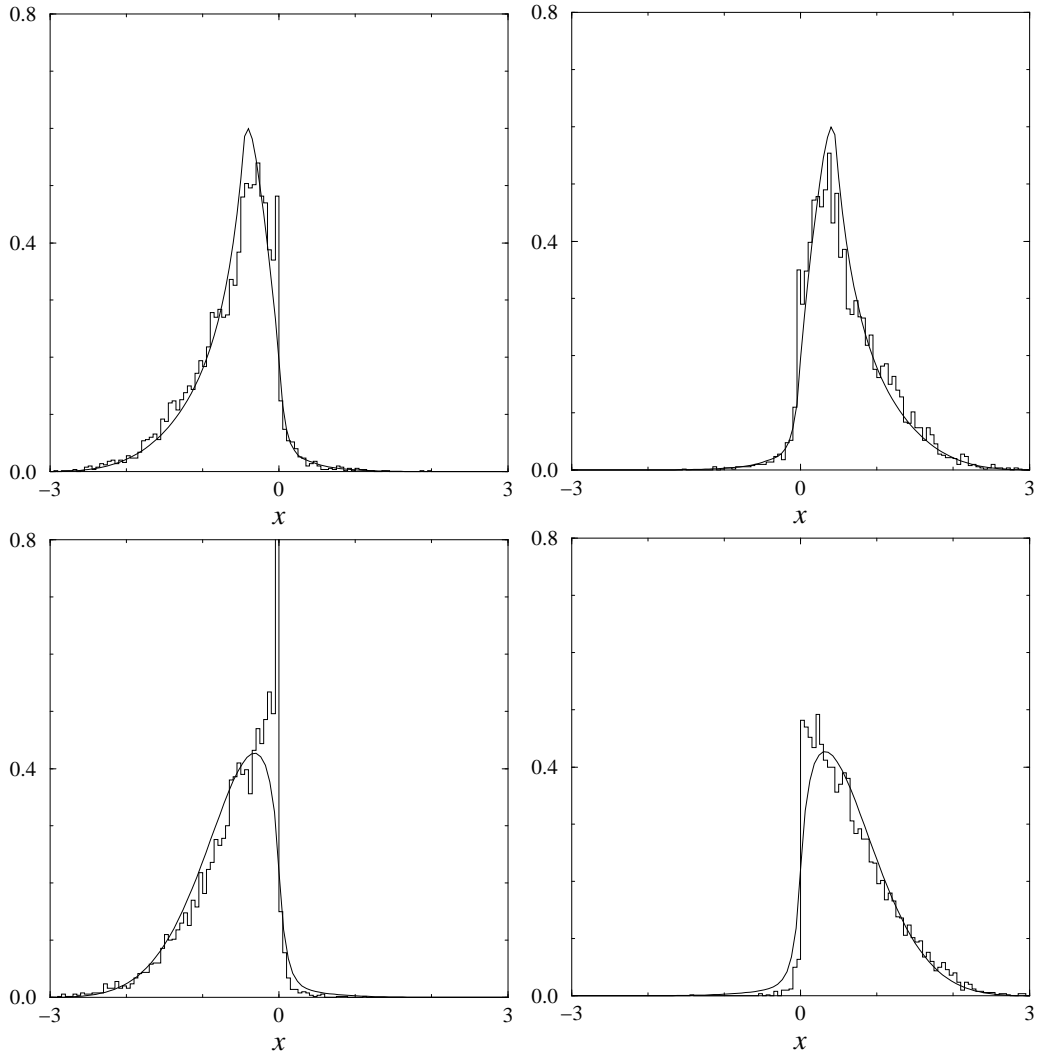


Figure 10: Comparison between the full numerical solution of our equations and the results of doing numerical simulations of on-line learning with $N = 10,000$ and $\alpha = 1$. Histograms: conditional student field distributions $P^\pm(x) = \int dy P[x, y]\theta[\pm y]$ as measured at time $t = 5$. Smooth curves: corresponding theoretical predictions. Upper pictures: Perceptron learning, with $\eta = 1$ (left: $P^-(x)$, right: $P^+(x)$). Lower pictures: AdaTron learning, with $\eta = \frac{3}{2}$ (left: $P^-(x)$, right: $P^+(x)$).

Our restricted resolution numerics obviously have difficulty in reproducing the discontinuous behaviour of $P^\pm(x)$ near $x = 0$ for on-line Adatron learning (as expected), which explains why in this regime the simplest large α approximation (which can be numerically evaluated with almost arbitrarily high field resolution) appears to outperform the more sophisticated versions of the theory (which CPU limitations force us to evaluate with rather limited field resolution), according to figure 9.

We conclude from the results in this section that our full theory indeed gives an adequate description of the macroscopic process, and that the partially annealed approximation is almost equivalent in performance to the full theory. As mentioned before, the conditionally-Gaussian approximation performs generally poorly (except, as we have seen earlier, for the simple Hebian rule). Which of the remaining three versions of our theory to use in practice will clearly depend on the accuracy constraints and available CPU time of the user, with the full theory at the higher end of the market (in

principle very accurate, but almost too CPU expensive to work out and exploit properly), with the large α approximation on the lower end (reasonably accurate, but very cheap), and with the annealed approximation as a sensible compromise in between these two.

6 Discussion

Our aim in this sequel paper was to work out the general theory developed in [1] for several supervised (on-line and batch, linear and non-linear) learning scenarios in single-layer perceptrons, to develop a number of systematic approximations from the full set of equations, and to test the theory and its approximations against both exactly solvable benchmarks and extensive numerical simulations. The theory, built on the dynamical replica formalism [2], was designed to predict the evolution of training- and generalisation errors, via a non-linear diffusion equation for the joint distribution of student and teacher fields, in the regime where the size p of the (randomly composed) training set scales as $p = \alpha N$, with $0 < \alpha < \infty$ and where N denotes the number of inputs. In this regime the input data will in due course be recycled, as a result of which complicated correlations develop between the student weights and the realisations of the data vectors (with their corresponding teacher answers) in the training set; the student fields are no longer described by Gaussian distributions, training- and generalisation errors will no longer be identical, and the more traditional and familiar statistical mechanical formalism as developed for infinite training sets consequently breaks down.

We have first worked out our equations explicitly for the special case of Hebbian learning, where the availability of exact results, derived directly from the microscopic equations, allows us to perform a critical test of the theory. For batch Hebbian learning we can demonstrate explicitly that our theory is fully exact. For on-line Hebbian learning, on the other hand, proving or disproving full exactness requires solving a non-trivial functional saddle-point equation analytically, which we have not yet been able to do. Nevertheless, we can prove that our theory is exact (i) with respect to its predictions for Q , R and E_g , (ii) with respect to the first moments of the conditional field distributions $P[x|y]$ (for any $y \in \mathbb{R}$), and (iii) in the stationary state. In order to also generate predictions for intermediate times we have constructed an approximate solution of our equations, which is found to describe the results of performing numerical simulations of on-line Hebbian learning essentially perfectly.

No exact benchmark solution is available for non-Hebbian (i.e. non-trivial) learning rules, leaving numerical simulations as the only yardstick against which to test our theory. Motivated by the need to solve a functional saddle-point equation at each time step in the full theory, and by the presence of nested integrations, we have constructed a number of systematic approximations to the original equations. We have compared the predictions of the full theory and of the three approximation schemes with one another and with the results obtained upon performing numerical simulations of non-linear learning rules, such as Perceptron and AdaTron, in large perceptrons (of size $N = 10,000$), with various values of learning rates η and relative training set sizes α . One of the approximations, a conditionally-Gaussian saddle-point approximation in the spirit of the particular approximation that was found to work perfectly for Hebbian learning, turned out to perform badly for general non-Hebbian rules. The other two approximations, the large α approximation and the partially annealed approximation, each have their specific usefulness; the former is extremely simple and fast, whereas the latter is overall more accurate, but more expensive in its CPU requirements (so that in practice its true accurateness cannot always be realised). Yet, the large α approximation still works remarkably well, even for small α , in spite of it being so simple that it can be written as a fully explicit set of equations for Q , R and the joint field distribution $P[x, y]$ only. For on-line learning these equations

can be simplified to

$$\begin{aligned}\frac{d}{dt}Q &= 2\eta\langle x\mathcal{G}[x,y]\rangle + \eta^2\langle\mathcal{G}^2[x,y]\rangle & \frac{d}{dt}R &= \eta\langle y\mathcal{G}[x,y]\rangle \\ \frac{d}{dt}P[x|y] &= \frac{1}{\alpha} \int dx' P[x'|y] \left\{ \delta[x-x'-\eta\mathcal{G}[x',y]] - \delta[x-x'] \right\} + \frac{1}{2}\eta^2 \frac{\partial^2}{\partial x^2} P[x|y] \langle\mathcal{G}^2[x',y']\rangle \\ &\quad - \eta \frac{\partial}{\partial x} \left\{ P[x|y] \left\langle \mathcal{G}[x',y'] \left[yy' + \frac{(x-\bar{x}(y))(\bar{x}(y')-Ry') + (x-Ry)(x'-\bar{x}(y'))}{Q-R^2} \right] \right\rangle \right\}\end{aligned}$$

with $\langle f[x,y] \rangle = \int Dydx P[x|y]f[x,y]$ and $\bar{x}(y) = \int dx xP[x|y]$. The observed accurateness of these simple equations in the small α regime suggests that for $\alpha \rightarrow 0$ the leading term in the diffusion equation for $P[x|y]$ is the first term in the right-hand side, which reflects the direct effect of pattern recycling, and which indeed has not been approximated.

For a discussion of further theoretical developments and refinements of the present dynamical replica formalism we refer to [1]. We believe that our theory offers an efficient tool with which to analyse and predict the outcome of learning processes in single-layer networks. In particular, for those who are primarily interested in the progress and the outcome of learning processes there is no real need to understand the full details of the derivation in [1]; as in this paper, one can simply adopt the macroscopic laws of [1] (or one of the two appropriate approximations, to save CPU time) as a starting point, and just apply them to the learning rules as hand. Generalization to multi-layer networks (with a finite number of hidden nodes) is straightforward, although numerically intensive [9]. The case of noisy teachers can also be studied with an appropriate extension of the present formalism [10], involving a joint distribution of three rather than two fields (namely those of student, ‘clean’ teacher, and ‘noisy’ teacher). In the example applications worked out so far in this paper (Hebbian learning, Perceptron learning and AdaTron learning) our formalism has been found to be either exact or an excellent approximation. It is not realistic to expect that simpler theories can be found with a similar level of accuracy. While putting the finishing touch to this manuscript a preprint was communicated [11] in which the authors apply the cavity method to the present problem. They manage to keep their theory relatively simple by restrict themselves in several serious ways (to batch learning only, and to gradient descent learning rules in order to use FDT relations) and by applying their theory only to a linear learning rule. Here also the present theory would have been both simpler and exact. An exact theory for both on-line and batch learning and for arbitrary learning rules can be constructed [12] using a suitable adaptation of the path integral methods as in [13], with the obvious appeal of full mathematical rigour at any time, but in describing transients it is going to be more complicated than the present one as it will be built around macroscopic observables with two time arguments rather than one (correlation- and response functions) and will take the form of an effective single weight process with a dynamics with coloured stochastic noise and retarded self-interactions.

Acknowledgement

DS and ACCC gratefully acknowledge support by the Engineering and Physical Sciences Research Council (grant GR/L52093) and by the London Mathematical Society (grant 4415).

References

- [1] Coolen ACC and Saad D 1999 *King's College London preprint KCL-MTH-99-32*
- [2] Coolen ACC, Laughton SN and Sherrington D 1996 *Phys. Rev. B* **53** 8184
- [3] Coolen ACC and Saad D 1998 in *On-Line Learning in Neural Networks* D. Saad (Ed) (Cambridge: U.P.)
- [4] Rae HC, Sollich P and Coolen ACC 1999 *J. Phys. A: Math. Gen.* **32** 3321
- [5] Kinzel W and Rujan P 1990 *Europhys. Lett.* **13** 473
- [6] Biehl M and Schwarze H 1992 *Europhys. Lett.* **20** 733
- [7] Kinouchi O and Caticha N 1992 *J. Phys. A: Math. Gen.* **25** 6243
- [8] Press WH, Flannery BP, Teukolsky SA and Vetterling WT 1988 *Numerical Recipes in C* (Cambridge: U.P.)
- [9] Coolen ACC, Saad D and Xiong YS 1999 *in preparation*
- [10] Mace CWH and Coolen ACC 1999 *to be published in Proc. NIPS*99*
- [11] Wong KY, Li S and Tong YW 1999 *preprint cond-mat/9909004*
- [12] Heimel JA and Coolen ACC 1999 *in preparation*
- [13] Horner H 1992 *Z. Phys.* **B86** 291; *Z. Phys.* **B87** 371